The New Explanation for the Superconductor

Ting-Hang Pei
Thpei142857@gmail.com

Abstract- The superconductor theory based on the electron pair is reviewed and several viewpoints are proposed. A demonstrated case reveals the speed of each electron in the electron pair at Fermi level about 1.82×10^6 *m*/*s* in Pb. However, the fastest longitudinal and transverse speeds of crystal waves in Pb at 0 K are 2.18×10^3 *m*/*s* and 1.29×10^3 *m*/*s* in [100] direction, respectively. It seems to be very hard even impossible that the mediated phonon can real-time transfer momentum and energy between two so high-speed and antiparallel-momentum electrons in the superconducting state. In this research, we focus on single electron based on the experiments of Transmission Electron Microscopy. The new fitting temperature-dependent model for the London penetration depth is proposed. This model is much better than the one- and two-gap models and matches three experimental data much well. Then it further gives the temperature-dependent effective electron mass for the Nb superconductor film. Finally, the expression for the resistivity is deduced which can explain why the resistance is almost zero in the superconductor. All these new results are obtained by using the concept of single electron.

Keywords: superconductor, electron pair, mediated phonon, London penetration depth, resistivity, effective electron mass, temperature-dependent

I. Introduction

Since the first superconductor, Hg, was found the critical temperature T_c at 4.153 K in 1911 [1], a lot of research has been done about the physical properties and their performances [1-7]. The progress of superconductor has revealed some high-temperature superconductors, such as $YBa_2Cu_3O_7$ with T_c=92 K [4,5], $Tl_2Ba_2Ca_2Cu_3O_{10}$ with T_c=125 K [3,4,6], and the very high temperature record H_2S with T_c=203 K at 150 GPa [8]. How to explain its physical phenomenon is still a developed region even it has passed one century.

In the past sixty years, the electron pair theory is thought success in the explanation of the low-temperature superconductor. The best condition for the electron pair is consisting of two electrons with antiparallel momentum and spins. According to this theory, Fe is thought as an inappropriate element for the superconductor compounds. Since the superconductor LaOFeP with T_c~4 K was found in 2006 [9], this early deduction was broken. The compound $La(O_{1-x}F_x)FeAs$ with x between 0.05 and 0.12 has found T_c=26 K [10]. Furthermore, this compound has found another superconductivity at T_c=43 K [11] significantly higher than the critical temperature

T_c=39 K of MgB_2 [12]. The superconductor $SmFeAsO_{0.85}$ even shows the critical temperature as high as 55 K [13]. It naturally implies that this theory is not suitable for explaining this kind of superconductor consisting of Fe. It makes us deeply think about the role of the electron pair and find another better way to explain the superconducting phenomenon.

II. The Problems About The Electron-Pair Theory In The Superconductor

The traditional electron-pair theory considers two electrons existing weak attractive interaction between them in the superconducting state and these two electrons are in the bounded state [5,6,14]. The electron pair appears in the range about $k_B T_c$ above the Fermi energy ε_F where k_B is the Boltzman constant. These two electrons combine with each other due to the exchange of phonon, and their total energy is slightly lower than the total energy of two free electrons. This phenomenon is thought physically that one electron causes the deformation of the positive ions in its vicinity and creates a mediated phonon. Through absorbing this mediated phonon, the other electron is affected by this deformation. In this picture, its binding energy of an electron pair at zero temperature is Δ. The energy $E_{\vec{k}}$ of single electron with wavevector $\vec{k}$ in the excited state is

$$E_{\vec{k}} = \sqrt{\varepsilon_{\vec{k}}^2 + \Delta^2}, \tag{1}$$

and the energy $\varepsilon_{\vec{k}}$ of quasi-electrons counted from the Fermi energy ε_F is

$$\varepsilon_{\vec{k}} = \frac{\hbar^2 k^2}{2m_e^*} - \varepsilon_F, \tag{2}$$

where m_e^* is the effective electron mass, $\hbar$ equals to $h/2\pi$, and h is the Planck's constant. The Hamiltonian for this superconducting electron system with the vibrating positive ions is [5,14,15]

$$H = H_{\substack{free \\ electron}} + H_{\substack{Coulomb \\ interaction}} + H_{\substack{free \\ phonon}} + H_{\substack{electron-phonon \\ interaction}}. \tag{3}$$

Through complicated canonical transformation [15], the original one can transfer to another form

$$H_{transfer} = H_{\substack{quasi \\ electron}} + H_{\substack{shielded \\ Coulomb \\ interaction}} + H_{\substack{dressed \\ phonon}} + H_{\substack{electron-phonon-electron \\ interaction}}. \tag{4}$$

It describes a process that an electron is scattered from the initial state $\vec{k}$ to the final state $\vec{k}'$ through the emission or absorption of a phonon with the wavevector $\vec{q}$. In the electron-pair theory, the best condition for the electron pair is that their momentum $\vec{k}$ and spin s are equal and antiparallel, and the two electrons move in the opposite

directions. From these descriptions, we might ask whether the phonon-exchanged process is a physical picture or just a quasi-physical one.

For example, the metal lead (Pb) has the superconducting critical temperature of 7.193 K [5] and its Fermi energy is 9.37 eV [1]. The speed v_F at ε_F for the bare electron is about

$$v/c = \sqrt{2\varepsilon_F/m_e c^2} = \sqrt{18.74/511000} \sim 1/164, \quad (5)$$

where c is the speed of light in the free space and the bare electron mass m_e is 0.511MeV/c^2 or 9.1*10^{-31} kg. It means that the speed of electron is very high and about 1.82x10^6 m/s or (1/164) c [1]. However, the propagation of the lattice wave relies on the vibration of ions and the speed of the phonon at Debye frequency is not as so high as the Fermi electron speed. The mediated phonon between two electrons is the acoustic phonon and the crystal wave can be approximated to the continuously elastic wave. For Pb, the elastic stiffness constant C_{11} is 0.555x10^{12} dyne/cm^2 and C_{44} is 0.194x10^{12} dyne/cm^2, and the density ρ is 11.599 g/cm^3 at 0 K [1]. The highest speed of the crystal wave is the longitudinal wave v_{LA} in [100] directions that is

$$v_{LA} = \sqrt{\frac{C_{11}}{\rho}} = 2.18 \times 10^3 \ m/s. \quad (6)$$

The speed of phonon is more 800 times slower than Fermi electron. Similarly, the speed of the transverse wave v_{TA} is

$$v_{TA} = \sqrt{\frac{C_{44}}{\rho}} = 1.29 \times 10^3 \ m/s, \quad (7)$$

which is about 1400 times slower than Fermi electron.

Next, the average distance between two electrons is necessary to estimate when considering the electron-pair picture. The electrons of each electron pair are within the range about $k_B T$ above the Fermi energy and the density of these electrons approximates

$$n k_B T_c/\varepsilon_F \sim 10^{29} \ \cdot 10^{-5} \ m^{-3} = 10^{24} \ m^{-3} \quad (8)$$

or $10^6/\mu m^3$ in Pb [1]. This kind of electron roughly occupies a cubic with size about 100 Å and it gives the average distance between two electrons about 100 Å or roughly 30~40 atoms. This is a long distance for such two electrons, and the mediated phonon has to cross several ten atoms from one electron to the other.

If one electron can absorb a mediated phonon bringing the changes of momentum and energy from the other electron, the propagation of this phonon has to be very fast. Actually, both electrons have so high speed so it is almost impossible to real-time exchange a phonon between two electrons across 100Å. Even it is possible, the electron much more probably absorbs other phonons prior to the mediated phonon due to other scattering events, caused from other electron-ion interactions or thermal vibrations. The

phonon is the quantization of the crystal wave and is the collective excitation. In other words, the wave can propagate through the whole crystal and each electron can absorb or scatter these phonons through the electron-phonon interaction. However, the electron pair means that the mediated phonon cannot propagate globally and only exists between two electrons for the purpose of exchanging momentum and energy.

Let's further look at the real picture for these two electrons. The original concept for the electron pair is shown in Fig. 1.The mediated phonon is created due to the distortion of ions in the vicinity of an electron. However, the electron-pair theory ignores that both electrons have ability to make ions distorted and induce respective crystal waves. It means that two phonons can be created simultaneously or successively so it is possible to exist more than one mediated phonons between two electrons, not always only one. In this theory, when one electron emits a phonon with momentum $\vec{q}$ and changes its momentum from $-\vec{k}$ to $-\vec{k}-\vec{q}$, then the other one absorbs this phonon and its momentum is changed from $\vec{k}$ to $\vec{k}+\vec{q}$. However, this process is non-conservation of energy and the mediated phonon should be virtual, not real one. Actually, the really possible process is that one electron emits a real phonon and changes its momentum from $-\vec{k}$ to $-\vec{k}-\vec{q}$ but the other electron doesn't be affected by this phonon, or absorb another real phonon $\vec{q}'$ and its momentum is changed from $\vec{k}$ to $\vec{k}+\vec{q}'$.

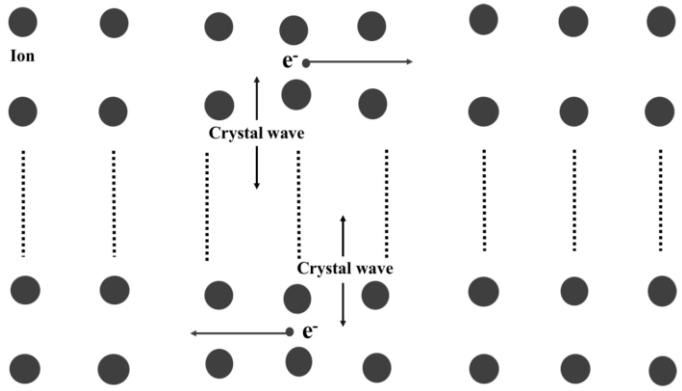

Fig. 1 An ideal case for a real electron pair 'bounded' by a phonon. According to the electron-pair theory, the ionic deformation in the vicinity of each electron causes a crystal wave propagating in the superconductor. Two electrons exchange a mediated phonon in an electron pair. The vertical dash lines in the central region means a distance between two electrons and a lot of atoms in between them. Their average distance is about 100 Å. However, this process is non-conservation of energy. The speed of Fermi electron can be 800-1400 times faster than the two fastest crystal waves in Pb. Actually, the speed of two electrons is so high that it is very hard even impossible to real time transfer a mediated phonon between them.

Next, we further consider another two electrons are added in Fig. 1 where each one of them is positioned close to each previous electron. Due to the distortion of the lattices, each electron in the electron pair creates the respective crystal wave and the two additional electrons can feel each crystal wave as shown in Fig. 2. However, the electron-pair theory only permits the crystal wave propagating between two electrons in an electron pair, so these two additional electrons cannot interact with these crystal

waves in principle. It makes such crystal waves unique and unphysical. As mention before, this theory restricts the crystal waves propagating locally, not globally.

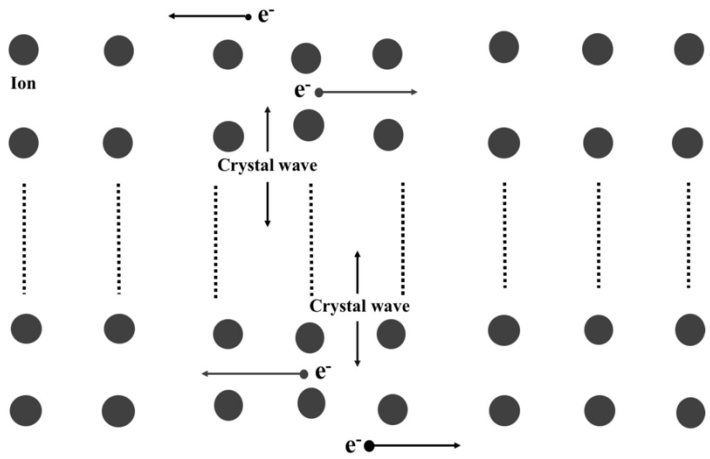

Fig. 2 Two more electrons are added on the top and bottom in Fig. 1. In the electron-pair theory, these crystal waves don't affect these additional electrons because the crystal wave only take responsibility to exchange momentum and energy between two electrons in Fig. 1. According to this picture, it seems to be very unreasonable when the crystal wave only propagates between two electrons.

Actually, the decrease in the electron energy for the electron pair shouldn't mean the existence of the effectively attractive interaction which take responsibility to form the electron pair. In the high-density electron gas, it also shows a negative perturbation energy in the random phase approximation (RPA)

$$\epsilon_k' = \frac{\hbar^2 k^2}{2m_e} - \Omega \int\limits_{|\vec{l}|<k_F} \frac{\hbar d\vec{l}}{(2\pi)^3} \frac{4\pi e^2}{\left[\left(\hbar\vec{k} - \hbar\vec{l}\right)^2 + \lambda^2\right]}. \tag{9}$$

The energy ϵ_k' of a quasiparticle at k near Fermi wavevector k_F is

$$\epsilon_k' = \frac{\hbar^2 k^2}{2m_e} - 0.166 r_s (\ln r_s + 0.203) \frac{\hbar^2 k k_F}{2m_e} + constant, \tag{10}$$

where

$$r_s = \frac{1}{a_0}\left(\frac{3}{4\pi n}\right)^{1/3} \tag{11}$$

and $a_0 = \hbar^2/m_e e^2$ is Bohr radius [15]. However, it has not yet been thought that the effectively attractive force also exist between electrons to arise the stable electron pair in the RPA calculations, similar to the electron-pair theory in the superconductor.

This electron-pair theory proposes the superconducting contributions from all electron pairs. In fact, the phonon can also be created from the thermal vibration. There are a lot of phonons with different frequencies coexisting in the superconductor. One electron can obtain the energy and momentum from absorbing phonons no matter where

they originally come from in the superconductor. Actually, this collective excitation or crystal wave created from the deformation of lattice can propagate to the wide place and is possibly absorbed by many electrons. It is alike a lot of speedboats moving on the sea and each of them creates propagating wave. Then each of those speedboats can receive waves from others, not only from certain one. It is very hard to restrict one boat receiving the wave from certain speedboat and excluding others in the open region.

The propagating wave caused by the speedboat is similar to the electrons and phonons in the superconductor. To restrict each electron in the electron pair only interacting with their mediated phonon is unphysical even this phonon is true. Especially when the superconductor has some imperfections like defects or disorders, we have to consider these effects because the calculations of the quasi-electron energy and m_e^* in Eq. (2) also necessarily consider the lattice structure including the imperfections. The imperfection is an important factor for resistance. The superconductor with a near periodic structure should have the critical temperature higher than the one with much random structure in it even both have the same constitution.

When we study the electron-pair theory, another question also arises. As we know, the normal electron current naturally exists in the superconductor. The normally electron current $\vec{J}_{sn}$ in the superconductor is

$$\vec{J}_{sn} = -\int_{\Delta}^{\infty} eN_S\left(E_{\vec{k}}\right) f\left(E_{\vec{k}}\right)\vec{v}_{\vec{k}} dE_{\vec{k}}, \tag{12}$$

where $f(E_{\vec{k}})$ is the Fermi-Dirac distribution, $-e$ is the electron charge, and $\vec{v}_{\vec{k}}$ is the electron velocity at wavevector $\vec{k}$. $N_s(E_{\vec{k}})$ is the density state of the normal electron in the superconductor

$$N_s(E_{\vec{k}}) = N(E_{\vec{k}})\frac{d\varepsilon_{\vec{k}}}{dE_{\vec{k}}} = N(E_{\vec{k}})\frac{E_{\vec{k}}}{\sqrt{E_{\vec{k}}^2 - \Delta^2}} \tag{13}$$

when $|E_{\vec{k}}| > \Delta$, and

$$N_S(E_{\vec{k}}) = 0 \tag{14}$$

when $|E_{\vec{k}}| < \Delta$. It is similar to the electric current $\vec{J}$ under the applied electric field $\vec{E}$ in the traditional metal which has the form

$$\vec{J} = n\frac{e^{*2}}{m_e^*}\tau\vec{E}, \tag{15}$$

where n is the average charge density, e^* is the effective charge, and τ is the average

scattering or relaxation time. However, these excited normally electrons should cause some resistivity as the electrons in the normal metals because of inelastic scatterings and energy dissipation. Since the normal electrons also exist in the superconducting state, it makes us think about why the resistance is still almost zero in the superconductor experiments. The resistivity ρ for the normal conductor has relationship with τ of the electron, that is

$$\rho \propto \frac{1}{\tau}. \tag{16}$$

It means that if the experiments show almost zero resistivity, the normally excited electron would have very large τ like a quasi-superconducting electron.

III. The Perfect Conductor

As we know, the single electron in the perfectly periodical or crystal structure is represented by the Bloch wave. It can have a stable solution that the electron propagates in the periodic structure near freely. The resistance is mainly created by the imperfect lattice and inelastic scattering with impurities. The dream conductor is the electron system with no dissipation in this perfect structure. It has been pointed out that the perfect conductor can shield electric and magnetic fields from its surface [16] so the Meissner effect and London penetration depth [2-4] may be explained by the traditional conductor theory. This is a reasonable explanation by using Pb as a demonstrated example. When the temperature is across T_c from low to high, the magnetic penetration depth in Pb should be continuous as the material state changes from the superconducting state to the normally metallic one.

In electrodynamics [16], the surface current $\vec{K}_s$ on the conductor is produced by the surface moving charges and the induced tangential magnetic field $\vec{H}$ is

$$\hat{n} \times \vec{H} = \vec{K}_s, \tag{17}$$

and Ohm's law gives $\vec{K}_s = \sigma \vec{E}_c$ with a finite conductivity σ for the electric field $\vec{E}_c$ in the conductor. Then we have the magnetic fields $\vec{H}_c$ inside the conductor is

$$\vec{H}_c = -\frac{ic}{\mu_c \omega} \nabla \times \vec{E}_c, \tag{18}$$

where μ_c is the permeability of the conductor. We also have the equation for $\vec{E}_c$

$$\vec{E}_c \approx \frac{c}{4\pi\sigma} \nabla \times \vec{H}_c. \tag{19}$$

The skin depth δ is

$$\delta = \left(\frac{2}{\mu_c \omega \sigma}\right)^{1/2}, \tag{20}$$

the electric field in the conductor

$$\vec{E}_c \approx \sqrt{\frac{\mu_c \omega}{8\pi\sigma}}(1-i)\left(\hat{n} \times \vec{H}\right) e^{-x/\delta} e^{ix/\delta}, \tag{21}$$

and the magnetic field in the conductor

$$\vec{H}_c = \vec{H} e^{-x/\delta} e^{ix/\delta}, \tag{22}$$

where x is the distance from the surface in the conductor. This equation is much similar to the magnetic field in the superconductor characterized by the London penetration depth. The time-average power loss P_{loss} per unit area a is

$$\frac{dP_{loss}}{da} = \frac{\mu_c \omega \delta}{4} \left|\vec{H}\right|^2. \tag{23}$$

Above equation shows that the energy loss is proportional to δ at a fixed frequency ω and a constant magnetic field. From Eq. (20), the larger σ is, the smaller is δ. The larger conductivity benefits the electric current and lowers power loss. Once the factors of dissipation are removed, the material can perform like a dream conductor as a superconductor. In the following, according to the above discussions, we think about an advanced way how to explain the superconductor with near zero resistance or resistivity. All the research focuses on one electron propagation in the superconductor.

IV. The Viewpoint From The Stopping Power In Transmission Electron Microscopy

Since the Transmission Electron Microscopy (TEM) was developed [17], the detailed structure for a lot of materials can be obtained in the nanoscale imaging. It also a good technology for investigating superconductors and their TEM images have been revealed for many years [18-27]. As we know, it is the relativistic electron used in TEM and the acceleration voltage can be as high as several hundred KeV [17]. When we discuss the imaging processes in TEM, it needs to consider the stopping power for different materials [17, 28-38]. It means that the electrons lose their energy when passing through the sample and it is unavoidable due to the inelastic scatterings between electrons and atoms. Especially, the secondary electrons would stop in the sample and transfer all their energy to the material. No matter what kind of the material is, the energy loss always exists. It is the same as the superconductor that we also have to calculate the stopping power when using TEM. The TEM experiments of superconductors reveal the existence of the electron energy loss definitely. Furthermore, TEM can provides the electron-energy-loss spectra of samples [17,39].

The TPP2-TM model [40-46] very successfully predicts the inelastic mean free path $\lambda_{\text{Inelastic}}$ in the material having close relationship with the incident energy E of an electron that is

$$\lambda_{Inelastic} = \frac{E}{E_p^2\{\beta \ln(\gamma E) - (C/E) + (D/E^2)\}} \text{ (in Å)}, \tag{24}$$

where $E_p = 28.8(N_v\rho/M)^{1/2}$ (in eV) is the free-electron plasma energy, N_v is the number of valence electrons per atom for solids or per molecule for compounds, ρ is the density (in g/cm^3), and M is the atomic or molecular weight. β, γ, C, and D are defined in Ref. 46 [46]. It is the modified Bethe equation and matches with the experimental data very well for many element solids, compounds, and molecules in some ranges of the incident electron energy [40-46]. As mentioned previously, the TEM imaging can show the inner structure of the superconductor due to the scattering from the incoming particles with inner atoms. It always accompanies with energy lost which implies the resistance in the superconductor until to very high voltage about several KeV. The stopping power has been studied many years. The well-known formula for the electron energy stopping power is the relativistically Bethe-Bloch equation [31], that is

$$-\frac{dE}{dx} = \frac{N_A\rho_m e^4 Z}{8\pi\epsilon_0^2 A m_e v^2}\left[\ln\left(\frac{E^2}{I^2}\frac{\gamma+1}{2}\right) + F(\gamma) - \delta_F(\gamma)\right], \tag{25}$$

$$F(\gamma) = \left[\frac{1}{\gamma^2} - \frac{2\gamma-1}{\gamma^2}\ln(2) + \frac{1}{8}\left(\frac{\gamma-1}{\gamma}\right)^2\right], \tag{26}$$

where E is the kinetic energy, x is the traveling distance, I is the mean excitation energy, $\gamma = 1/\sqrt{1-v^2/c^2}$, v is the speed of the incident electron, $\delta_F(\gamma)$ is the density correction, N_A is the Avogadro's constant, A is the atomic weight, Z is the atomic number, and ρ_m is the mass density. We can ignore the radiation stopping power because it is only significant when the atomic number Z>80 and the electron energy E>10 MeV. For the low-energy case, γ~1. Then above equation for the compound becomes

$$-\frac{dE}{dx} = \frac{N_A\rho_m e^4}{8\pi\varepsilon_0^2 m_e v^2}\sum_i c_i\frac{Z_i}{A_i}\ln\left(\frac{E}{I_i}\right)\left(\frac{\text{eV}}{\text{Å}}\right), \tag{27}$$

where A_i is the ith-element atomic weight, I_i is the ith—element mean excitation energy, Z_i is the ith-element atomic number, and c_i is the ratio of the ith-element in the compound. From Eq. (27), it reveals that small Z_i/A_i benefits the electron holding its kinetic energy and the stopping power becomes small. The larger I_i also results in the smaller stopping power.

Now, considering an experiment to measure the current of the superconductor as shown in Fig. 3. An electron gun is positioned above the superconductor thin film in

vacuum. It is similar to the traditional way which the normal metallic wire contacts the superconductor to form a closed loop but here the superconductor is under zero bias. The collecting plate behind the superconductor film can receive most passing electrons including the secondary electrons. The benefit of this experimental setup is to replace the concept of the electron pair with the single electron inside the superconductor. Due to the focus on the movement of the single electron, it makes us use a different viewpoint to initially discuss why the resistance is so small in the superconductor.

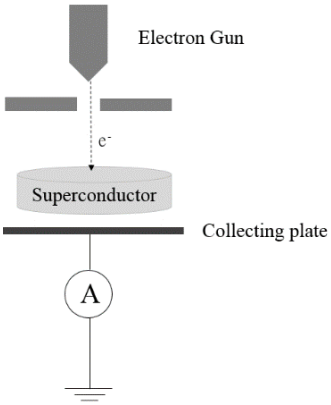

Fig. 3 The simple experimental setup for measuring the electric current A of the superconductor thin film. The electric voltage is applied on the electric gun to emit electrons.

From the Joule's heat law, the electric power dissipation is equal to I^2R where I is the electric current and R is the resistance. If we consider the electron energy loss is proportional to I^2R, then the resistance is also proportional to the electron energy loss. When the critical temperature T_c is defined as the resistance less than a certain value, then T_c can be the function of $1/R$ or $1/|dE/dx|$. According to Eq. (27), it seems to be able to quantitatively explain that $Bi_2Sr_2Ca_2Cu_3O_{10}$ (110 K) has T_c higher than $YBa_2Cu_3O_7$ (92 K), $Tl_2Ba_2Ca_3Cu_4O_{11}$ (122 K) is higher than $Bi_2Sr_2Ca_2Cu_3O_{10}$ (110 K), and $HgBa_2Ca_2Cu_3O_8$ (133 K) is higher than $Tl_2Ba_2Ca_3Cu_4O_{11}$ (122 K) [5,7].

Although the standard measurement of the superconductor current is not like the experimental setup in Fig. 3, however, TEM experiments clearly exhibit the single-electron transmission through the superconductor. It is almost impossible to find a conduction electron with energy of several keV in the superconductor to form an electron pair with the incident electron. Especially the velocity of the electron is close to c. This gives a reasonable way to discuss the resistance of the superconductor by the single-electron viewpoint.

V. The Correction Model For The Resistivity Varying With Temperature

Next, another simple schematic picture for measurements of the electrical current and resistance of the superconductor is shown in Fig. 4. In the traditional theory for conductor, the electrical conductivity σ is defined as [1]

$$\sigma = \frac{ne^2\tau}{m_e^*}. \tag{28}$$

It obeys the relation $\vec{j} = \sigma\vec{E}$ as Eq. (15) where $\vec{j}$ is the electrical current density and $\vec{E}$ is the electrical field. The electrical resistivity ρ is the reciprocal of the electrical conductivity σ [1]. As we know, the electrical resistivity of metal is the function of the temperature T [1], that is,

$$\rho \propto T^5. \tag{29}$$

The resistance R has relationship with the resistivity ρ. For a conductor wire, $R=\rho L/A$ where L is the length and A is the cross-section area. The discussion of ρ is a good way to know the behavior of R.

The Kondo effect explains the magnetic ion-conduction electron interaction resulting in additional spin-dependent resistivity in solute magnetic alloys [1]. The electrical resistivity has the form

$$\rho = aT^5 + \eta\rho_0 + \eta\rho_1 \ln T, \tag{30}$$

where a is a constant, η is the concentration, ρ_0 is the measure of the strength of the exchange scattering, $\rho_1 = 3\rho_0 z I_e/\varepsilon_F$, z is the number of the nearest neighbors, and I_e is the exchange energy. The other possible resistivity source is from the Umklapp process. The Umklapp scattering of electrons by phonons has significant contribution to the electrical resistivity when the Fermi surface is close to the zone boundary. The number of phonons for this kind of scattering process decreases as $\exp(-\hbar\omega_m/k_B T)$ where $\hbar\omega_m$ is the phonon energy. The expression of resistivity has to be improved when it applies on the superconductor.

The concept of the quasi-electron tells us that the electron mass needs to be corrected because of the high-density electron gas and ion background. The dependence of the effective electron mass on temperature T should also appear in the electrical resistivity especially at low temperature. According to the temperature dependence of the electron mobility in the semiconductor, the temperature-dependent electron mobility μ_e is

$$\mu_e = \frac{e}{m_e^*\left(AT^{3/2} + \frac{BN_i}{T^{3/2}}\right)} \tag{31}$$

where A and B are constants, and N_i is the impurity density [47]. The first term of the bracket in the denominator is due to the acoustic phonon scattering and the second one is due to the impurity scattering. Comparing this equation with μ_e experiments [47], it further reveals that m_e^* is also dependent on temperature with the form

$$m_e^*(T) = m_e^*(T_{ref})f(T), \tag{32}$$

where $f(T)$ is an undetermined function of temperature T and the reference of effective electron mass is chosen at some reference temperature T_{ref}, for example, T_{ref}=300 K. In addition, the energy gaps of Si and GaAs [47] also exhibit temperature dependence which means the calculations of the effective electron mass from the energy band dependent on temperature.

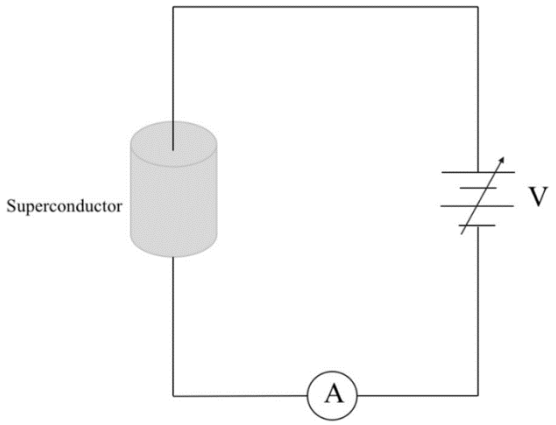

Fig. 4 Another simple electric circuit setup for measuring the electric current A and the resistance or resistivity of the superconductor. The electric voltage V is directly applied on the superconductor.

If we further use the temperature-dependent effective electron mass to the electrical conductivity for superconductor in Eq. (29), the electrical resistivity is expressed as

$$\rho(T) = aT^5[f(T)]^v. \tag{33}$$

As we know, the electrical resistance and resistivity near the critical temperature has dramatical decrease, so $f(T)$ can be chosen as an increasing function of T and v is a real value. Because the electrical resistance of superconductor is defined less than 10^{-19} ohm, the electrons in superconductor are much low energy loss and almost freely, and they have very long mean free path. It also means only the phonons with very small energy $\hbar\omega$ participating the electron-phonon interaction so the electron energy loss from the electron-phonon interaction is very small.

Except for these long-wavelength excited phonons, the Umklapp scattering is the other consideration in the calculation of the electrical resistivity, and then we have another form similar to Eq. (33), that is,

$$\rho(T) = aT^2[f(T)]^v \int \frac{d\omega}{2\pi} \frac{1}{exp\left(-\frac{\hbar\omega}{k_B T}\right) - 1}, \tag{34}$$

where $\hbar\omega << k_B T$. The electrons at or above Fermi energy take responsibility for the electrical conduction and the Fermi surface is very close to the zone boundary. Because the Umklapp scattering is considered, the total number of phonons is changed from T^3 to the exponential term in Eq. (34). Both equations make sure that the electrical resistivity is small enough at low temperature in the superconductor.

VI. The London Penetration Depth At Low Temperature

Since the effective electron mass is temperature-dependent as shown in Eq. (32), first of all, the function $f(T)$ has to be found out. According to London's theory [3], the penetrating depth λ_L in the superconducting state is

$$\lambda_L(T) = \sqrt{m_e^*/\mu_0 n_s e^{*2}}, \tag{35}$$

where n_s is the density of the superelectron above Fermi energy, μ_0 is the magnetic permeability in free space, and e^* is the effective charge of the superelectron. It is proportional to $(m_e^*/n_s)^{1/2}$ and has another expression the so-called two-fluid empirical model [2-4]

$$\lambda_L(T) = \lambda_0 \left[1 - \left(\frac{T}{T_c}\right)^4\right]^{-1/2}, \tag{36}$$

where $\lambda_0=\lambda_L(0)$ is the London penetration depth at absolute zero temperature.

The London temperature-dependent penetration depth has been widely studied and different fitting models proposed. Some methods for measurements have been used for a long period, such as self-oscillating tunnel diode resonator [48] and two-coil mutual-inductance technique [49]. The very early report showed that the results of the experiments on pure Sn [50] have some departure from the temperature-dependent penetration depth in Eq. (36). Recently, a lot of experiments about the change of the London penetration depth $\Delta\lambda_L(T) = \lambda_L(T) - \lambda_L(0)$ have been measured. According to the report, the experimental values $\Delta\lambda_L(T)$ of single crystal Y-Ba-Cu-O are between the two-fluid model and weak-coupling electron-pair theory [51]. The fitting function $\Delta\lambda_L(T)$ at low temperature is often well described by the power law of $\Delta\lambda_L(T) = bT^n$ where b is a constant and the range of n is often between 1 and 3 or even higher values [52-70]. According to $\Delta\lambda_L(T)$, the London penetration depth is $\lambda_L(T) = \lambda_0 + bT^n$ [58]. However, it should be finite at $T=T_c$. The magnetic penetration depth is not infinite actually. Some experiments have shown the finite value $\lambda_L(T)$ at T_c which are much more reasonable than Eq. (36) [58,62,63,65-70].

Then we discuss the range of n from the experimental fittings at low temperature. The fit for Y-Ba-Cu-O single crystal is changed from n=2 to n=1 when the temperature is cross the characteristic temperature T^* [55,56]. Some Y-Ba-Cu-O thin films show the power law fits with n from 1.4 to 2.2 [57]. It even mentioned that there was no way to obtain satisfactory exponential fit to these experimental data. The best fits for the non-magnetic PCCO single crystals are n=2.25±0.01 for one sample and n=2 for the other two samples [58]. For the magnetic NCCO single crystal, the best fits are n=1.35±0.03 and n=1.40±0.03 for different Curie constant [58]. The Sr_2RuO_4 single crystals show n~2 and n~3 [59]. The fits of LaFePO single crystals give n=1.2±0.1 for T<1 K [60].

The fitted n of $Ba(Fe_{1-x}Co_x)_2As_2$ single crystals with different x value varies from 2.0±0.1 for the underdoped samples to 2.5±0.1 for the overdoped samples [61]. Especially, single crystals of $Ba(Fe_{0.93}Co_{0.07})_2As_2$ were observed n=2.4±0.1 [65]. Two hole-doped iron-based superconductors of $Ba_{0.55}K_{0.45}Fe_2As_2$ and $Ba_{0.7}K_{0.3}Fe_2As_2$ single crystals have n=2 at low temperature [62]. Single crystals of $RFeAsO_{0.9}F_{0.1}$ (R=La,Nd) have been studied for possessing non-exponential London penetration depth [63]. The mean T_c is 45 K for La-1111 and 14 K for Nd-1111 where the power law of in-plane $\Delta\lambda_L(T)$ gives n=2 at low temperature. The low-temperature $\Delta\lambda_L(T)$ of iron-pnictide and iron-chalcogenide superconductors were studied and there were six superconductor samples giving n between 1.7 and 2.5 [67]. Other iron-chalcogenide superconductors $Fe_{1.03}(Te_{0.63}Se_{0.37})$ and $Fe_{1.06}(Te_{0.88}S_{0.14})$ were also reported $\Delta\lambda_L(T)$ with n~2.1 for Fe(Te, Se) and n~1.8 for Fe(Te,S) [68]. For single crystals of electron-doped $Ba(Fe_{1-x}Ni_x)_2As_2$, the results show the temperature dependence for different doping level [66]. It gives in-plane $\Delta\lambda_L(T)$ with $n \geqq 2$ for the optimal doping level and n<2 in the overdoped regime at low temperature. The interplane $\Delta\lambda_L(T)$ is T linear behavior below $T_c/3$ in the overdoped regime. The in-plane $\Delta\lambda_L(T)$ in single crystals of $Ba(Fe_{1-x}T_x)_2As_2$ (T=Co, Ni) irradiated with $^{208}Pb^{56+}$ ions exhibits 2.2<n<2.8 [69]. The London Penetration Depth in iron-based superconductors have ever reported n as high as 2.83 [70].

The other often used fitting function is the weak-coupling electron-pair or gap model including the exponential term shown as

$$\Delta\lambda_L(T) = \lambda_0 \sqrt{\frac{\pi\Delta}{2T}} exp\left(-\frac{\Delta}{T}\right), \tag{37}$$

where Δ is the value of the energy gap for the electron pair used in Eq. (1) and it doesn't satisfy the low T/T_c region in the most reports. Some reports show the inconsistent exponential behavior compared with the experimental data and the power law is better than this exponential model, such as UBe_{13} [53], Y-Ba-Cu-O single crystal [55,56], Y-Ba-Cu-O thin film [57], non-magnetic PCCO single crystal [58], magnetic NCCO single crystal [58], $Ba(Fe_{1-x}Co_x)_2As_2$ single crystal near optimal dipping of x=0.074 [61,70], $Ba(Fe_{0.93}Co_{0.07})_2As_2$ single crystal [65], and $(Ba_{1-x}K_x)Fe_2As_2$ single crystal with x=0.45 [58].

Except for the low-temperature region, the exponential behavior also not always fits the high-temperature region near T_c [62,63]. It clearly shows that the superfluid density of R-1111 crystals decreases slowly close to T_c where the exponential behavior approximates a straight line. The deviation means that the exponential behavior is not suitable for the high-temperature region near T_c in this studying case. Even the two-gap exponential model cannot also fit some experiments very well at the temperature close to T_c [62,63]. This model exhibits large errors comparing with experimental data even

in the high T/T_c region when λ_0=1400 Å [54]. As discussed previously, the electron pair is not real physical phenomenon so the reasonableness of the gap model is a doubted problem.

However, from the fitting functions in these references [52-70], the power law is not so accurate for all temperature range below T_c. Sometime, in the low-temperature region n is one value but it changes to other value above T^* [55]. The fast increase in $\Delta\lambda_L$ as T close to T_c means that this one-term power law doesn't satisfy in the high T/T_c region. We have to add more high power terms to fit the experimental data. For example, the magnetic penetration depth of c-axis oriented $YBa_2Cu_3O_7$ has also been reported [51] where the function matches well the experimental data

$$\lambda_L(T,H) = \frac{(\Phi_0 H)^{1/2}}{\pi^{1/2} H_c(0)} \left[1 - 2\left(\frac{T}{T_c}\right)^2 + \left(\frac{T}{T_c}\right)^4\right]^{-1/2}, \quad (38)$$

where H is the applied magnetic field, Φ_0 is the quantum flux, and $H_c(0)$ is the critical magnetic field at 0 K. It is clear that the sign associated with T^4 is different from Eq. (36). Furthermore, comparing Eq. (38) with Eq. (36), there is an additional T^2 term. It means that Eq. (36) for the London penetration depth would be better by adding some different T-order terms. Furthermore, considering the continuum at T_c and $\lambda_L(T_c)$ is finite so Eqs. (36) and (38) need to be improved for the superconductors.

VII. The New Fitting Model For The London Penetration Depth

Those superconductors for experiments [52-70] including single crystal, polycrystalline, pure, and dirty samples. The two fluid mode described by Eq. (36) also has something to do with the surface energy and the free energy of the superconductor. It is very reasonable that we physically add more T-order terms in the two-fluid model to fit the experimental data in the wide temperature range. This correction in London penetration depth includes T, T^2, T^3, and T^5 terms for considering the range of n values in the power law [52-70], that is,

$$\lambda_L(T) = \lambda_0 \left[1 - c_4\left(\frac{T}{T_c}\right)^4 - c_1\left(\frac{T}{T_c}\right)^1 - c_2\left(\frac{T}{T_c}\right)^2 - c_3\left(\frac{T}{T_c}\right)^3 - c_5\left(\frac{T}{T_c}\right)^5\right]^{-1/2}, \quad (39)$$

where c_1, c_2, c_3, c_4, and c_5 are constants determining from the curve fitting and all of them between -1.0 and 1.0 in our calculations. This choice makes sure the low-temperature behavior predicting by the power law and the high-temperature behavior which the electron-pair model cannot describe very well. Although those fitting values of n in the power law show it less than 4.0 [52-70], however, it is better to include T^5 term in the curve fittings. Then we choose three experimental data to investigate how

much the improvement of Eq. (39) is.

First, we consider the 70-nm thickness Nb superconducting film [71]. Here without considering the electron-pair coherent length and Pippard Kernal, we find that their experimental data can be fitted much well by Eq. (39) above $0.5T_c$. According to experiments, this Nb film gives the London penetration depth λ_0 about 112 nm and it would be at least several times larger than λ_0 at T=T_c. Then we use the final seven data closest to T_c to get the better fitting curve. The experimental data and the fitting cure of $\lambda_L^2(0)/\lambda_L^2(T)$ varying with T/T_c are shown in Fig. 5(a) where c_1=0.28, c_2=-0.63, c_3=0.97, c_4=0.99, and c_5=-0.63 are used. This fitting result is even better than the very complicated Pippard kernel integral. Especially in the high-temperature region, the Pippard Kernel integral shows large deviations with the experimental data.

The second case is the experimental data of $\lambda_L^2(0)/\lambda_L^2(T)$ in the superconductor $YBa_2Cu_3O_{6.95}$ with T_c>93 K [56]. We use all the experimental data with λ_0=1500 Å in the range of T/T_c between 0.0 and 1.0 to fit the curve. These data show strong linear behavior at low temperature. Then choosing c_1=0.54, c_2=-0.28, c_3=0.62, c_4=-0.88, and c_5=0.99 in Eq. (39), the fitting curve matches the experimental data much better than the *s*-wave electron-pair model as shown in Fig. 5(b). From low to high temperature, the fitting curve almost match the experiment at each data. Only the final data closest to T_c has some deviation but it is still within the experimental error. This fitting curve perfectly describes this experimental trend and it gives the London penetration depth about 10 λ_0 at T_c.

The third case is the single-crystalline $Fe_{1.03}(Te_{0.63}Se_{0.37})$ superconductor with T_c~12 K and λ_0~560 nm [68]. The whole experimental data are used to get the fitting curve. The experimental data and the fitting curve by using Eq. (39) are both shown in Fig. 5(c). It gives c_1=0.27, c_2=0.99, c_3=0.99, c_4=-0.90, and c_5=-0.38 from the fitting. The results also show the fitting curve almost matching each experimental data except for final three data closest to T_c. Furthermore, this fitting curve is much better than the two-gap γ model which has explicit deviation at low-temperature region until to $0.4T_c$ [68]. In summary, these three cases reveal the gap model less accurate and Eq. (39) can fit the experiments fairly well.

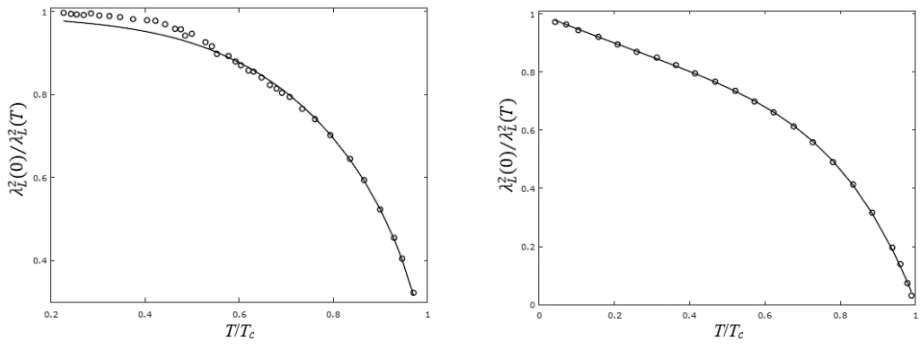

(a) (b)

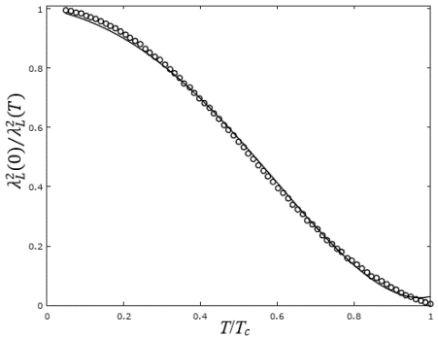

(c)

Fig. 5 (a) $\lambda_L^2(T)/\lambda_L^2(0)$ of the 70-nm thickness Nb superconductor film is drawn varying with T/T_c. Circles are the experimental data [71] and solid line is the fitting curve with c_1=-0.63, c_2=0.99, c_3=0.97, c_4=-0.63, and c_5=0.28 in Eq. (42). (b) The fitting curve (solid line) and experimental data (circle) for $\lambda_L^2(T)/\lambda_L^2(0)$ with λ_0=1500 Å [56]. In this case, c_1=0.54, c_2=-0.28, c_3=0.62, c_4=-0.88, and c_5=0.99. The fitting curve is fairly good in this case. (c) The fitting curve (solid line) and experimental data (circle) for $\lambda_L^2(T)/\lambda_L^2(0)$ in the third case [68]. Here c_1=0.27, c_2=0.99, c_3=0.99, c_4=-0.90, and c_5=-0.38 are used in this fitting curve and the fitting result is much well.

VIII. The Expression For The Effective Electron Mass

After verifying Eq. (39) by three cases of different superconductors very well, then the next step is to substitute Eq. (39) into Eq. (35) to get the relation

$$\frac{m_e^*(T)}{\mu_0(T)n_s(T)e^{*2}(T)} = \lambda_0^2 G(T), \tag{40}$$

where the function at the right-hand side is

$$G(T) = \left[1 - c_1\left(\frac{T}{T_c}\right)^1 - c_2\left(\frac{T}{T_C}\right)^2 - c_3\left(\frac{T}{T_c}\right)^3 - c_4\left(\frac{T}{T_c}\right)^4 - c_5\left(\frac{T}{T_c}\right)^5\right]^{-1}. \tag{41}$$

When we consider e^* as a constant value and the superconductor is non-magnetic for the most cases, then Eq. (46) can be reduced to

$$\frac{m_e^*(T)}{n_s(T)} = \mu_0 e^{*2}\lambda_0^2 G(T), \tag{42}$$

where $\mu_0(T)$=μ_0 in the considering temperature range. This treatment reasonably supposes two temperature-dependent terms n_s and m_e^*, and other quantities temperature-independent. The superconductivity has been found dependent on temperature and the environment pressure [72]. The effective electron mass m_e^* definitely also depends on temperature and pressure. When the material cools down, the lattice constant changes. The pressure also causes the same result. For example, the hydrogen phase diagram reveals different hydrogen phase varying with temperature and pressure [73]. The metallic hydrogen has been found at solid state under very high pressure [74]. Furthermore, H_2S can perform superconductivity at T_c=203 K under 150 GPa [8]. It is clear that the crystal structure is affected by temperature and the ultra-

high pressure so do the electronic band structure as well as the effective electron mass.

Then we try to get the function $f(T)$ in Eqs. (32) – (34). Considering the free-electron gas model for some metals in the superconducting state, it gives the density of state $g(E)$ is

$$\mathrm{g}(E) = 2\pi V_c \left(\frac{2m_e^*}{h^2}\right)^{3/2} \sqrt{2E}, \tag{43}$$

where V_C is the volume of the solid. Then the density of the superelectrons is

$$n_s = 2 \times 2\pi \left(\frac{2m_e^*}{h^2}\right)^{3/2} \int_{\mu}^{\infty} \frac{\sqrt{2E}}{exp\left(\frac{E-\mu}{k_B T}\right) + 1} dE. \tag{44}$$

Here we still consider the superelectron obeying the Fermi-Dirac distribution because it is single-electron model, not consisting of double electrons. When the concept of the quasi-electron is used, the electron mass m_e is also replaced with m_e^* in Eqs. (43) and (44). The chemical potential μ is a temperature-dependence quantity [75] expressed as

$$\mu(T) \approx \varepsilon_F \left[1 - \frac{\pi^2}{12}\left(\frac{k_B T}{\varepsilon_F}\right)^2\right]. \tag{45}$$

Substituting Eq. (45) into Eq. (44), it gives

$$n_s(T) \approx \frac{2\pi^3}{3}\left(\frac{2m_e^*}{h^2}\right)^{3/2} \frac{1}{\sqrt{2\varepsilon_F}} (k_B T)^2. \tag{46}$$

Then substituting Eq. (46) into Eq. (42) and adopting $e^*=e$, it gives

$$\frac{2\pi^3 e^2 \mu_0}{3h^3} (2m_e^*)^{1/2} \frac{1}{\sqrt{2\varepsilon_F}} (k_B \lambda_0)^2$$

$$= \frac{1}{T^2}\left[1 - c_1\left(\frac{T}{T_c}\right)^1 - c_2\left(\frac{T}{T_c}\right)^2 - c_3\left(\frac{T}{T_c}\right)^3 - c_4\left(\frac{T}{T_c}\right)^4 - c_5\left(\frac{T}{T_c}\right)^5\right]. \tag{47}$$

After rearranging it, then we have

$$m_e^*(T) = m_0\left[\left(\frac{T_c}{T}\right)^2 - c_1\left(\frac{T_c}{T}\right)^1 - c_2 - c_3\left(\frac{T}{T_c}\right)^1 - c_4\left(\frac{T}{T_c}\right)^2 - c_5\left(\frac{T}{T_c}\right)^3\right]^2, \tag{48}$$

where

$$m_0 = \frac{9h^6 \varepsilon_F}{4\pi^6 e^4 \mu_0^2 k_B^4 \lambda_0^4 T_c^4}. \tag{49}$$

Eq. (48) combined with Eq. (49) can give $m_e^*(T) > 0$ for $T<T_c$.

In order to get $m_e^*(T)$ for $T>T_c$ and the continuity at $T=T_c$, $m_e^*(T)$ for $T>T_c$ near

the critical temperature can be expressed as

$$m_e^*(T) = m_0\left[\left(\frac{T}{T_c}\right)^2 - c_1\left(\frac{T}{T_c}\right)^1 - c_2 - c_3\left(\frac{T_c}{T}\right)^1 - c_4\left(\frac{T_c}{T}\right)^2 - c_5\left(\frac{T}{T_c}\right)^3\right]^2. \quad (50)$$

According to Eqs. (48) and (50), the value $log_{10}(m_e^*(T)/m_0)$ varying with T/T_c is calculated for Nb superconductor film as shown in Fig. 6(a). The effective electron mass of Nb is $m_e^* = 12m_e$ [2] and Fig. 6(a) gives the value about 0.99 at 273 K. We can choose m_0=12m_e in this case and the calculations give m_e^* almost equal to 12m_e at $T > 3T_c$.

Actually, the value $m_e^*(T)/m_0$ below T_c seems to close the heavy electron superconductors. Several superconductors with very heavy effective electron mass have been reported [5]. UBe_{13} has critical temperature T_c=0.85 K, $CeCu_2Si_2$ has T_c=0.65 K, and UPt_3 has T_c=0.54 K. URu_2Si_2 is also reported T_c=1.2 K [4]. Their effective electron mass is two or three orders of magnitude larger than the normal electron mass. However, Eq. (48) has a singularity at T=0 which is unreasonable and needs to be removed. When we multiply a temperature–dependent correct term at the right-hand side, the value seems to reasonably fit $m_e^*(T) < m_e$ for a lot of superconductors. This correction term is $(T/T_c)^{4+\xi}$ so Eq. (48) becomes

$$\frac{m_e^*(T)}{m_0} = \left(\frac{T}{T_c}\right)^{4+\xi}\left[\left(\frac{T_c}{T}\right)^2 - c_1\left(\frac{T_c}{T}\right)^1 - c_2 - c_3\left(\frac{T}{T_c}\right)^1 - c_4\left(\frac{T}{T_c}\right)^2 - c_5\left(\frac{T}{T_c}\right)^3\right]^2. \quad (51)$$

where ξ is zero or a small quantity. This correction might be due to the superelectron density $n_s(T)$ in Eq. (46) which is temperature independent or weak temperature dependent and their number is different from the nearly free electron in the normal metal. The different choice of ξ results in different curve below T_c. When considering the behavior at T very close to zero, ξ=0 is a good choice. If Eq. (46) represents the standard electron density above Fermi surface in the normal metal, it means that the electron gas in the superconductor would be the high-density system for T_c > 1 K and the low-density one for T_c < 1 K. For some superconductors with T_c > 1 K, the superelectron gas would be the high-density system. The probability of the electron-phonon interaction is dramatically decrease with temperature in both Eqs. (33) and (34), so the material performs superconductivity. This reason also may explain why some good conductors, such as Ag, Cu, Au, I-A and II-A metals in the periodic element table, have not been found superconductivity because of their low-density superelectron gas.

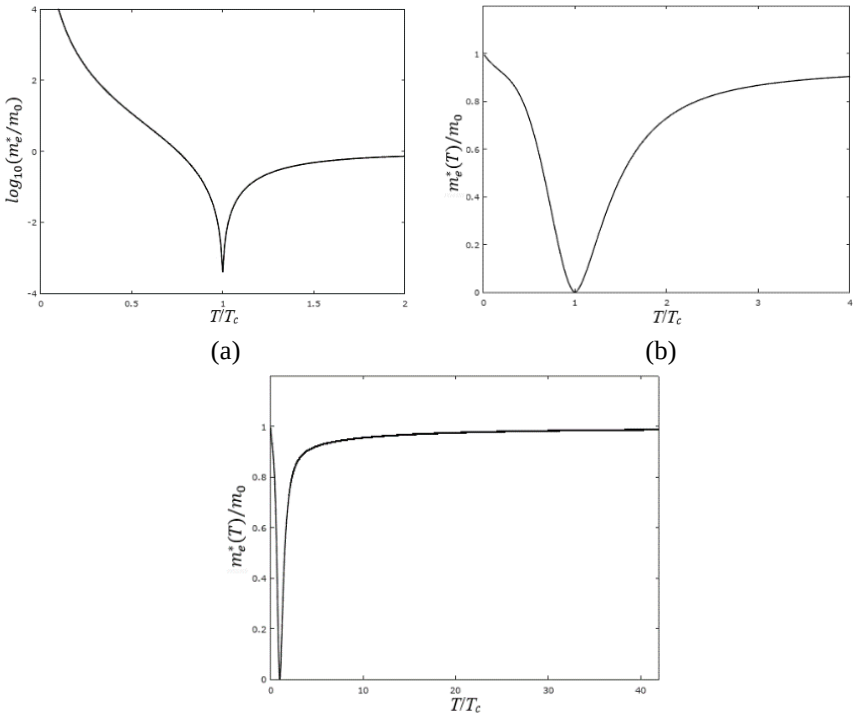

Fig. 6 (a) Calculations of $log_{10}(m_e^*/m_0)$ varying with T/T_c according to Eqs. (48) and (50). (b) Calculations of (m_e^*/m_0) varying with T/T_c after multiplying a temperature correction term in Eq. (51) with ξ=0. (c) The much longer temperature range of (m_e^*/m_0) calculated by Eq. (51) with ξ=0.

IX. The Single-Electron Resistivity Of The Superconductor

Finally, we can use Eqs. (51) and (50) to deduce the resistivity in the Nb superconductor film. The function $f(T)$ of the resistivity in Eqs. (33) and (34) can be obtained according to Eq. (51) and Eq. (50), that is,

$$f(T) = m_0 \left(\frac{T}{T_c}\right)^{4+\xi} \left[\left(\frac{T_c}{T}\right)^2 - c_1\left(\frac{T_c}{T}\right)^1 - c_2 - c_3\left(\frac{T}{T_c}\right)^1 - c_4\left(\frac{T}{T_c}\right)^2 - c_5\left(\frac{T}{T_c}\right)^3\right]^2$$

$$for\ T < T_c, \tag{52}$$

and

$$f(T) = m_0 \left[\left(\frac{T}{T_c}\right)^2 - c_1\left(\frac{T}{T_c}\right)^1 - c_2 - c_3\left(\frac{T_c}{T}\right)^1 - c_4\left(\frac{T_c}{T}\right)^2 - c_5\left(\frac{T}{T_c}\right)^3\right]^2$$

$$for\ T_c < T. \tag{53}$$

In Eq. (34), the electron-phonon interaction should be weak enough. It is reasonable because the strong electron-phonon interaction can take more energy away from the electron. Low temperature lowers the phonon excitation and therefore the energy dissipation decreases. Substituting Eqs. (52) and (53) into Eqs. (33) and (34), and supposing $\hbar\omega = bk_BT_c$ where b is a constant, then we have the temperature-dependent resistivity for normal process

$$\rho(T) = aT^5[f(T)]^v, \tag{54}$$

and for the Umklapp process

$$\rho(T) = aT^2[f(T)]^v \frac{1}{exp\left(b\frac{T}{T_c}\right) - 1}. \tag{55}$$

Here the integration in Eq. (34) is replaced with an average number distribution. According to Eqs. (54) and (55), two cases for the compact temperature-dependent resistivity $\rho(T)/a\, m_0^v$ of the Nb superconductor film varying with T/T_c are drawn in Fig. 7(a). Here ξ in Eq. (52) is chosen as zero. The curve described by T^5 for the normal metal is also shown in Fig. 7(a). v=1 are used for both equations and b=0.50 is used in Eq. (55). In Fig. 7(a), two cases described by Eqs. (54) and (55) exhibit the compact resistivity much lower than the T^5 curve in the vicinity of T_c. Then the log10 of the compact resistivity is also calculated for these three equations as shown in Fig. (b) where T/T_c varies from 1.0 to 3.0. It explicitly shows very sharp decreases near T_c for both Eqs. (54) and (55). The T^5 curve changes smoothly and is three orders higher than the other two equations. Eqs. (54) and (55) can extend to many superconductor cases and reasonably explain the sharp decreases of the resistivity near T_c. Although the calculations of Eqs. (54) and (55) are a little larger than the T^5-calculations at around T/T_c=0.70, all of them are still much smaller than it is at $T>T_c$.

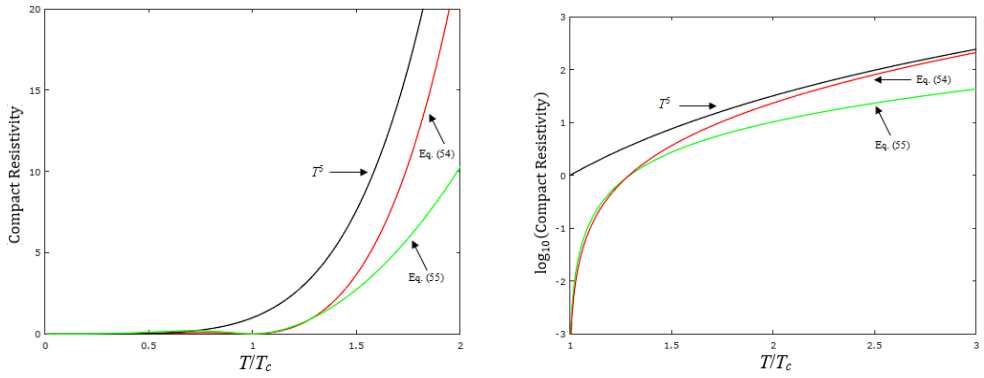

(a) (b)

Fig. 7 (a) Compact resistivity varying with T/T_c for two cases described in Eqs. (54) and (55) for the Nb-superconductor film [71] where v=1.0 in Eqs. (54) and (55), and b=0.50 in Eq. (55). (b). $\log_{10}$(Compact Resistivity) varying with T/T_c for these three equations from T/T_c=1.0 to T/T_c=3.0. The parameters v and b are the same as (a).

The resistivity model can be improved by considering the parameters (v, b) are different in the different temperature region and b is a temperature-dependent function. For example, about the Umklapp process, it is

$$\rho(T) = aT^2[f(T)]^v \frac{1}{exp\left(b(T)\frac{T}{T_c}\right) - 1}. \tag{56}$$

The temperature-dependent parameter b comes from the effect of phonons because the exponential term is original from Eq. (34) where the entire phonon contributions are considered. Therefore, the exponential term in Eq. (57) can be thought as the average effect of the whole photons and it is temperature-dependent naturally. We find an simple and appropriate expression of $b(T)$ to be

$$b(T) = b_0 \frac{T}{T_c}. \tag{57}$$

Of course, it is possibly a complicated series which includes some high-order T-terms, but Eq. (56) with Eq. (57) can be good enough to satisfy some experiments. The transition metal and alloy normal-state resistivity is related to the phonons. The T^3 low-temperature dependence of resistivity has been reported for an Nb magnetron-sputtered film at least to 29.5 K [76], in which the equation of the dashed line representing the normal-state resistivity in Fig. 1 is approximated to

$$\rho(T) - \rho_0 \cong \frac{3.0}{2.9} \times 10^{-5}(T^3 - 10^3) \quad (\mu\Omega \cdot cm/K^3), \tag{58}$$

where the normal-state resistivity at 10 K is ρ(10 K)$\cong\rho_0$. If we use the normal-state resistivity at 10 K to be a reference, then Eq. (58) tells us that the cubic root of the increasing resistivity starting from ρ(10 K) is very close to $0.0218T$ $(\mu\Omega \cdot cm)^{1/3} \cdot$K. Therefore, the cubic root of the increasing normal-state resistivity performs linearity in T. In order to satisfy this report, our model is also respected for the similar behavior performing the T^3 low-temperature dependence of resistivity in the normal state. Next, we choose appropriate parameters in Eqs. (56) and (57). The parameters (v, b) is obviously in the normal state different from those in the superconducting state because the performances of phonons and electrons are very different in these two states. Thus, we show a case by choosing two different parameters (v, b) in the normal and superconducting states, respectively. In the superconducting state, v_1=1.0 and b_0=b_1=30.0, and in the normal state, v_2=0.22 and b_0=b_2=2.50. The cubic root of the normalized resistivity calculated by Eqs. (56) and (57) is shown in Fig. 8(a) from 0 K up to $3T_c$, in which the normalized resistivity is defined as $\bar{\rho}(T) = \rho(T)/\rho(1.01T_c)$. This temperature range coves both the superconducting and normal states and the transition temperature range from the superconducting state to the normal state is about $0.01T_c$. For the Nb superconductor, the critical temperature T_c=9.5 K [1], then the maximum temperature shown in Fig. 8(a) is about 28.5 K, close to the 1995 report about the Nb normal-state resistivity in the low temperature [76]. In the meanwhile, a dashed line behaving the T^3 low-temperature dependence is also shown to n Fig. 8(a). It explicitly shows the curve calculated by Eqs. (56) and (57) matching better and better

the dashed line above $1.01T_c$ so our model not only shows extremely low resistivity in the superconducting state, but also the T^3 low-temperature dependence of resistivity in the normal state. Especially, the dashed line is almost coincident with the curve above $2.0T_c$. The slop of the dashed line is 1.0 in our calculation. Because we use the normalized resistivity in the y-axis, the curve is scalable when we compare the model with the experimental data. In Fig. 8(b), the normalized resistivity from 0 K to $3T/T_c$ is shown in the log scale where the normalized resistivity of the superconducting state is about 10^{-16} to 10^{-12}. In Eq. (57), we can choose different b_0=b_2 in the normal state, then we can discuss the effect of b_2 on the normalized resistivity. When b_2=0.45, the calculation shows the normalized resistivity about one order of magnitude higher than that of the b_2=0.25 case. However, both different b_2 cases almost not affect the normalized resistivity in the normal state. Therefore, the different b_2 mainly affects the normalized resistivity in the superconducting state. In summary, above discussions means that our model can explain the extremely low resistivity in the superconductor as well as the metallic resistivity in the normal state.

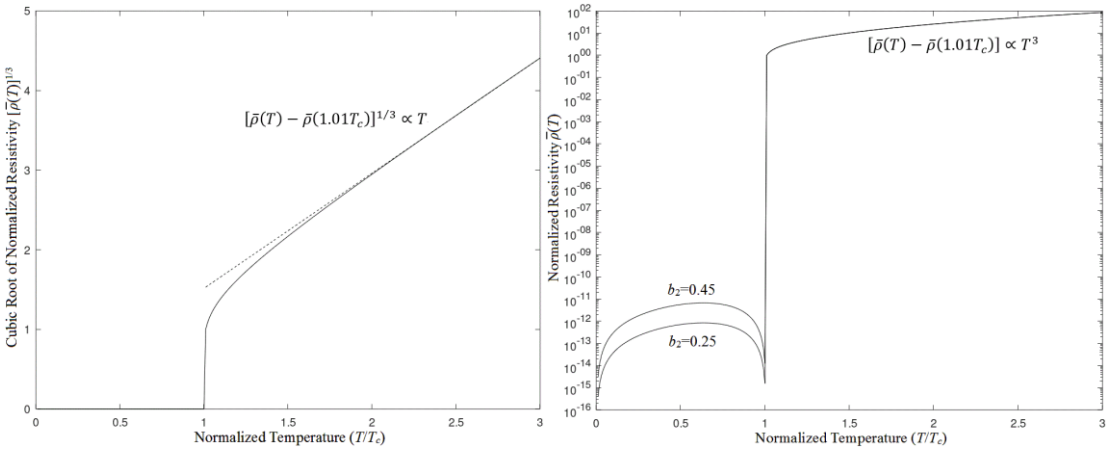

Fig. 8 (a) The model for the Umklapp process to describe the Nb resistivity in the low-temperature region from 0 K to $3T_c$. In this case, we use v_1=1.0 and b_1=30.0 at $T<T_c$, and v_2=0.22 and b_2=2.50 at $T\geq T_c$. The cubic root of the normalized resistivity shows extremely low resistivity in the superconducting state and T^3 low-temperature dependence of resistivity in the normal state which revealed in an Nb sputtered film in 1995 [76]. (b) The semi-log plot of the model for the Umklapp process describing the Nb resistivity in the low-temperature region. Two different b_2 cases show the effect on the normalized resistivity. The normalized resistivity is between 10^{-16} and 10^{-12} for the b_2=0.25 case and that between 10^{-15} and 10^{-11} for the b_2=0.45 case in the superconducting state, and it is almost not affected by these two b_2 in the normal state.

X. Conclusions

In conclusion, the electron pair in the superconducting state is a not real physical phenomenon because the velocity of the Fermi electron is several hundred to thousand faster than the crystal wave and the mediated phonon in this process is virtual. How to combine two high-speed electrons through a much slow mediated phonon is very hard even impossible to carry out. Especially, the phonon is the collective excitation and

many electrons have possibility to scatter or absorb the mediated phonon through the electron-phonon interaction. The mediated phonon should not only interact with two electrons and the weakly negative perturbation energy should not mean the possibility to form a stable electron pair in the superconductor. In RPA calculations, it has already revealed the negative energy correction for the quasi-electron in the high-density electron gas but it hasn't yet been considered a stable electron-pair picture there.

According to these discussions, we propose the single-electron viewpoint to explain the almost zero resistance or resistivity in the superconductor. The TEM experiments provide a good support that the energy loss exists when the several keV electron passes through the superconductor. It is almost impossible for a conduction electron in the superconductor to form an electron pair with the incident electron. Then we build the resistivity of the superconductor including the correction of the temperature-dependent effective electron mass. In the following, the correction function is tried to find out. Next, a new fitting model for the London penetration depth in the superconductor is first proposed. This new model can match three different superconductor experiments much better than the exponential electron-pair model. The later often has large deviations at low and high temperature. It further exhibits the finite London penetration depth at T_c which have been verified by some experiments.

Finally, the successful fitting model gives the collection function of the temperature-dependent effective electron mass for the resistivity of the superconductor. Using the fitting parameters from the experiment of the Nb superconductor film, the calculation results show the sharp decreases for the compact resistivity described by Eqs. (54) and (55) which is the characteristic of the resistivity near the critical temperature T_c for the superconductor. In the following, we use different parameters (v,b) in the superconducting and normal states for Eqs. (6) and (57) and finally, the normalized resistivity curve shows extremely low resistivity in the superconducting state and the T^3 low-temperature dependence of resistivity in the normal state which is coincident with the experiments of an Nb sputtered film in 1995 [76]. The results tell us that the high-density superelectron gas would be better for the existence of superconductivity and the electron-phonon interaction is very weak in the superconductor. When electron inelastically scatters the ion to produce a phonon, the small phonon energy results in the tiny energy lost taking away from an electron. It benefits the electron to hold most of its energy and therefore, the dissipation and resistivity are almost zero in the superconducting state.

AUTHOR'S CONTRIBUTIONS

All authors contributed equally to this work.

ACKNOWLEDGEMENTS

DATA AVAILABLE

The data that support the findings of this research are openly available in Materials Cloud at http://doi.org/10.24435/materialscloud:c2-5a.

References:

[1]. Charles Kittel, *Introduction to Solid State Physics* (John Wiley & Sons, Inc., 7th ed., 1996).

[2]. Charles P. Poole, Jr., Horacio A. Farach, and Richard J. Creswick, *Superconductivity* (Academic Press, Inc., San Diego, 1995).

[3]. Shu-Ang Zhou, *Electrodynamics of Solids and Microwave Superconductivity* (John Wiley & Sons, Inc., New York, 1999).

[4]. Kristian Fossheim and Asle Sudbo, *Superconductivity-Physics and Applications* (John Wiley & Sons, Inc., West Sussex, 2004).

[5]. James D. Patterson and Bernard C. Bailey, *Solid-State Physics*: *Introduction to the Theory* (Springer, Heidelberg, 2007).

[6]. Giuseppe Grosso and Giuseppe Pastori Parravicini, *Solid State Physics* (Academic Press, San Diego, 2000).

[7]. Efthimios Kaxiras, *Atomic and Electronic Structure of Solids* (Cambridge, Cambridge, 2003).

[8]. A. P. Drozdov, M. I. Eremets, I. A. Troyan, V. Ksenofontov, and S. I. Shylin, "Conventional superconductivity at 203 kelvin at high pressures in the sulfur hydride system," *Nat*. **525**, 73 (2015).

[9]. Yoichi Kamihara, Hidenori Hiramatsu, Masahiro Hirano, Ryuto Kawamura, Hiroshi Yanaji, Toshio Kamiya, and Hideo Hosono, "Iron-Based Layered Superconductor: LaOFeP," *J. Am. Chem. Soc*. **128**, 10012 (2006).

[10]. Yoichi Komihara, Takumi Watanabe, Masahiro Hirono, and Hideo Hosono, "Iron-Based Layered Superconductor [La($O_{1-x}F_x$)FeAs] (x=0.05-0.12) With T_c=26 K," *J. Am. Chem. Soc*. **130**, 3296 (2008).

[11]. Hiroki Takahashi, Karumi Igawa, Kazunobu Arii, Yoichi Kamihara, Masahiro Hirono, and Hideo Hosono, "Superconductivity At 43 K In An Iorn-Based Layered Compound $LaO_{1-x}F_xFeAs$," *Nat*. **453**, 376 (2008).

[12]. J. Nagamatsu, N. Nakagawa, T. Muranaka, Y. Zenitani, and J. Akimitsu, "Superconductivity at 39 K in magnesium diboride," *Nat.* **410**, 63 (2001).

[13]. Zhi-An Ren, Guang-Can Che, Xiao-Li Dong, Jie Yang, Wei Lu, Wei Yi, Xiao-Li Shen, Zheng-Cai Li, Li-Ling Sun, Fang Zhou and Zhong-Xian Zhao, "Superconductivity And Phase Diagram In Arsenic-Oxides ReFeAsO1-delta (Re=Rare-Earth Metal) Without Fluorine Doping," *Euro. Phys. Lett*. **83**, 17002 (2008).

[14]. Otfried Madelung, *Introduction to Solid-State Theory* (Springer, 3rd ed., New York, 1996).

[15]. Richard D. Mattuck, *A Guide to Feynman Diagrams in the Many-Body Problem* (Dover, 2nd Ed., New York, 1992).

[16]. J. D. Jackson, *Classical Electrodynamics* (John Wiley & Sons, 2nd ed., Singapore, 1990).

[17]. L. Reimer H. Kohl, T*ransmission Electron Microscopy – Physics of Image Formulation* (Springer, 5th ed., 2008).

[18]. A. Schilling, M. Cantoni, J. D. Guo, and H. R. Ott, "Superconductivity Above 130 K in The Hg-Ba-Ca-Cu-O System," *Nat.* **363**, 56 (1993).

[19]. Z. K. Tang, Lingyun Zhang, N. Wang, X. X. Zhang, G. H. Wen, G. D. Li, J. N. Wang, C. T. Chan, and Ping Sheng, *Sci*. **292**, 2462 (2001).

[20]. X. H. Zeng, A. N. Pogrebnyakov, A. Kotcharov, J. E. Jones, X. X. Xi, E. M. Lysczek, J. M. Redwing, S. Y. Xu, Q. Li, J. Lettieri, D. G. Schlom, W. Tian, X. Q. Pan, and Z. K. Liu, "*In Situ* Epitaxial MgB_2 Thin Films For Superconducting Electronics," *Nat*. *Mat*. **1**, 35 (2002).

[21]. S. X. Dou, S. Soltanian, J. Horvat, X. L. Wang, S. H. Zhou, M. Ionescu, H. K. Liu, P. Munroe, and M. Tomsic, "Enhancement of the critical current density and flux pinning of superconductor by nanoparticle SiC doping," *Appl*. *Phys*. *Lett*. **81**, 3419 (2002).

[22]. Thomas. E. Weller, Mark Ellerby, Siddharth S. Saxena, Robert P. Smith, and Neal T. Skipper, "Superconductivity In The Intercalated Graphite Compounds C_6Yb and C_6Ca," *Nat*. *Phys*. **1**, 39 (2005).

[23]. N. Reyren, S. Thiel, A. D. Caviglia, L. Fitting Kourkoutis, G. Hammerl, C. Richter, C. W. Schneider, T. Kopp, A.-S. Rüetschi, D. Jaccard, M. Gabay, D. A. Muller, J.-M. Triscone, J. Mannhart, "Superconducting Interfaces Between Insulating Oxides," *Sci*. **317**, 1196 (2007).

[24]. A. Gozar, G. Logvenov, L. Fitting Kourkouits, A. T. Bollinger, L. A. Gianuzzi, D. A. Muller, I. Bozovic, "High-Temperature Interface And Superconductivity Between Metallic And Insulating Cuprates," *Nat*. **455**, 782 (2008).

[25]. Athena S. Sefat, Michael A. McGuire, Brian C. Sales, Rongying Jin, Jane Y. Howe, and David Mandrus, "Electron Correlations In Superconductor $LaFeAsO_{0.89}F_{0.11}$ with Low Carrier Density," *Phys*. *Rev*. *B* **77**, 174503 (2008).

[26]. T. M. McQueen, A. J. Williams, P. R. Stephens, J. Tao, Y. Zhu, J. Ksenofontov, F. Casper, C. Felser, and R. J. Cava, "Tetragonal-to-Orthornombic Structural Phase Transition at 90 K In The Superconductor $Fe_{1.01}Se$," *Phys*. *Rev*. *Lett*. **103**, 57002 (2009).

[27]. Z. Wang, Y. J. Song, H. L. Shi, Z. W. Wang, Z. Chen, H. F. Tian, G. F. Chen, J. G. Guo, H. X. Yang, and J. Q. Li, "Microstructure And Ordering of Iron-Vacancies In The Superconductor System $K_yFe_xSe_2$ As Seen via Transmission Electron Microscopy," *Phys*. *Rev*. *B* **83**, 140505(R) (2011).

[28]. Athena S. Sefat, Michael A. McGuire, Brian C. Sales, Rongying Jin, Jane Y. Howe, and David Mandrus, "Electronic correlations in the superconductor $LaFeAsO_{0.89}F_{0.11}$ with low carrier density," *Phys*. *Rev*. *B* **77**, 174503 (2008).

[29]. K Kanaya and S Okayama, "Penetration and energy-loss theory of electrons in solid targets," *J*.

Phys. *D*: *Appl*. *Phys*. **5**, (1972).

[30]. J. C. Ashley, "Energy-loss probabilities for electrons, positrons, and protons in condensed matter," *J*. *Appl*. *Phys*. **69**, 674-678 (1991).

[31]. A. P. Sorini, J. J. Kas, J. J. Rehr, M. P. Prange, and Z. H. Levine, "*Ab initio* calculations of electron inelastic mean free paths and stopping powers," *Phys*. *Rev*. *B* **74**, 165111 (2006).

[32]. M. J. Berger and S. M. Seltzer, *Stopping Powers and Ranges of Electrons and Positrons* (2nd ed., 1982).

[33]. National Research Council (U.S.), *Nuclear Science Series Report Number 39*: *Studies in Penetration of Charged Particles in Matter*, (U. S. National Academy of Sciences, N. W., 1964).

[34]. J. F. Ziegler, *Handbook of Stopping Cross-Sections for Energetic Ions in All Elements* (Pergamon Press, 1980).

[35]. Donald E. Groom, Nikolai V. Mokhov, Sergei I. Striganov, and IHEP, Protvino, Russia, "Muon Stopping Powers And Ranges Of Electron And Positron," *Atomic Data and Nuclear Data Tables* **76**, LBNL-44742 (2001).

[36]. D. Emfietzoglou, I. Kyriakou, I. Abril, R. Garcia-Molina, and H. Nikjoo, "Inelastic scattering of low-energy electrons in liquid water computed from optical-data models of the Bethe surface," *Int*. *J*. *Radiat*. *Biol*. **88**, 22 (2012).

[37]. Dominique Drouin, Alexandre Re´al Couture, Dany Joly1, Xavier Tastet, Vincent Aimez, Raynald Gauvin, "CASINO V2.42-A Fast And Easy-to-Use Modeling Tool for Transmission Electron Microscopy And Microanalysis Users," *Scanning* **29**, 92 (2007).

[38]. Z. Francis, S. Incerti, M. Karamitros, H.N. Tran, C. Villagrasa, "Stopping power and ranges of electrons, protons and alpha particles in liquid water using the Geant4-DNA package," *Nucl*. *Instrum*. *Meth*. *Phys*. *Res*. *B* **20**, 2307 (2011).

[39]. R F Egerton, "Electron energy-loss spectroscopy in the TEM," *Rep*. *Prog*. *Phys*. **72**, 016502 (2009).

[40]. S. Tanuma, C. J. Powell, D. R. Penn, "Calculations of electron inelastic mean free paths for 31 materials," *Surf*. *Interface Anal*. **11**, 577-589 (1988).

[41]. S. Tanuma, C. J. Powell, and D. R. Penn, "Calculations of Electron Inelastic Mean Free Paths for 31 Materials," *Surf*. *Interface Anal*. **11**, 577 (1988).

[42]. S. Tanuma, C. J. Powell, and D. R. Penn, "Calculations of Electron Inelastic Mean Free Paths II. Data for 27 Elements over the 50-2000 eV Range," *Surf*. *Interface Anal*. **17**, 911 (1991).

[43]. S. Tanuma, C. J. Powell, and D. R. Penn, "Calculations of Electron Inelastic Mean Free Paths III. Data for 15 Inorganic Compounds over the 50-2000 eV Range," *Surf*. *Interface Anal*. **17**, 927 (1991).

[44]. S. Tanuma, C. J. Powell, and D. R. Penn, "Calculations of Electron Inelastic Mean Free Paths (IMFPs) IV. Evaluation of Calculated IMFPs and of the Predictive IMFP Formula TPP-2 for Electron Energies between 50 and 2000 eV," *Surf*. *Interface Anal*. **20**, 77 (1993).

[45]. S. Tanuma, C. J. Powell, and D. R. Penn, "Calculations of Electron Inelastic Mean Free Paths. V. Data for 14 Organic Compounds over the 50-2000 eV Range," *Surf*. *Interface Anal*. **21**, 165 (1994).

[46]. S. Tanuma, C. J. Powell, and D. R. Penn, "Calculations of Electron Inelastic Mean Free Path

(IMFPs). VII. Reliability of The TPP-2M IMFP Predictive Equation," *Surf. Interface Anal*. **35**, 268 (2003).

[47]. Donald A. Neamen, *Semiconductor Physics And Devices* (Richard D. Irwin, Inc., Burr Ridge, 1992).

[48]. Craig T. Van Degrift, "Tunnel diode oscillator for 0.001 ppm measurements at low temperatures," *Rev*. *Sci*. *Instrum*. **46**, 599 (1975).

[49]. A. T. Fiory and A. F. Hebard, "Penetration depths of High T_c films measured by two-coil mutual inductances," *Appl*. *Phys*. *Lett*. **52**, 2165 (1988).

[50]. A. L. Schavlow and G. E. Devlin, "Effect of The Energy Gap on The Penetration Depth of Superconductors," *Phys*. *Rev*. **113**, 120 (1959).

[51]. P. L. Gammel, A. F. Hebard, C. E. Rice, and A. F. J. Levi, "Temperature and Field Dependence Of The Magnetic Penetration Length Of C-Axis Oriented $YBa_2Cu_3O_7$ Films," *Phys*. *C* **162-164**, 1565 (1989).

[52]. F. Gross, B.S. Chandrasekhar, D. Einzel, K. Andres, P.J. Hirschfeld, H.R. Ott, J. Beuersl, Z. Fisk, and J.L. Smith, "Anomalous Temperature Dependence of the Magnetic Field Penetration Depth in Superconducting UBe_{13}," *Z*. *Phys*. *B – Condens*. *Matter* **64**, 175 (1986).

[53]. D. Einzel, P. J. Hirschfeld, F. Gross, B. S. Chandrasekhar, K. Andres, H. R. Ott, J. Beuers, Z. Fisk, and J. L. Smith, "Magnetic Field Penetration Depth in the Heavy-Electron Snyerconductor UBe_{13}," *Phys*. *Rev*. *Lett*. **56**, 2513 (1986).

[54]. L. Krusin-Elbaum, R. L. Greene, F. Holtzberg, A. P. Malozemoff, and Y. Yeshurun, "Direct Measurment of the Temperature-Dependent Magnetic Penetration Depth in Y-Ba-Cu-O Crystals," *Phys*. *Rev*. *Lett*. **62**, 217 (1989).

[55]. Peter J. Hirschfeld and Nigel Goldenfeld, "Effect of Strong Scattering in the Low-Temperature Penetration Depth of A d-wave Superconductor," *Phys*. *Rev*. *B* **48**, 4219 (1993).

[56]. W. N. Hardy, D. N. Bonn, D. C. Morgan, Ruxin Liang, and Kuan Zhang, "Precision measurements of the temperature dependence of λ in $YBa_2Cu_3O_{6.95}$: Strong evidence for nodes in the gap function," *Phys*. *Rev*. *Lett*. **70**, 3999 (1993).

[57]. A. Fuchs, W. Prusseit, P. Berberich, and H. Kinder, "High-precision penetration-depth measurement of YBa2Cu3O7-δ as a function of oxygen content," *Phys*. *Rev*. *B* **53**, R14745 (1996).

[58]. R. Prozorov, R.W. Giannetta, P. Fournier, and R. L. Greene, "Evidence for Nodal Quasiparticles in Electron-Doped Cuprates from Penetration Depth Measurements," *Phys*. *Rev*. *Lett*. **85**, 3700 (2000).

[59]. I. Bonalde, Brian D. Yanoff, M. B. Salamon, D. J. Van Harlingen, E. M. E. Chia, Z. Q. Mao, and Y. Maeno, "Temperature Dependence of the Penetration Depth in Sr_2RuO_4: Evidence for Nodes in the Gap Function," *Phys*. *Rev*. *Lett*. **85**, 4775 (2000).

[60]. J. D. Fletcher, A. Serafin, L. Malone, J. G. Analytis, J.-H. Chu, A. S. Erickson, I. R. Fisher, and A. Carrington, "Evidence for a Nodal-Line Superconducting State in LaFePO," *Phys*. *Rev*. *Lett*. **102**, 147001 (2009).

[61]. R. T. Gordon, C. Martin, H. Kim,1 N. Ni, M. A. Tanatar, J. Schmalian, I. I. Mazin, S. L. Bud'ko, P. C. Canfield, and R. Prozorov, "London penetration depth in single crystals of $Ba(Fe_{1-x}Co_x)_2As_2$

spanning underdoped to overdoped compositions," *Phys. Rev. B* **79**, 100506 (R) (2009).

[62]. C. Martin, R. T. Gordon, M. A. Tanatar, H. Kim, N. Ni, S. L. Bud'ko, P. C. Canfield, H. Luo, H. H. Wen, Z. Wang, A. B. Vorontsov, V. G. Kogan, and R. Prozorov, "Nonexponential London penetration depth of external magnetic fields in superconducting $Ba_{1-x}K_xFe_2As_2$ single crystals," *Phys. Rev. B* **80**, 020501 (R) (2009).

[63]. C. Martin, M. E. Tillman, H. Kim, M. A. Tanatar, S.K. Kim, A. Kreyssig, R. T. Gordon, M. D. Vannette, S. Nandi, V. G. Kogan, S. L. Bud'ko, P. C. Canfield, A. I. Goldman, and R. Prozorov, "Nonexponential London Penetration Depth of FeAs-Based Superconducting $RFeAsO_{0.9}F_{0.1}$ (R=La, Nd) Single Crystals," *Phys. Rev. Lett.* **102**, 247002 (2009).

[64]. A. B. Vorontsov, M. G. Vavilov, and A. V. Chubukov, "Superfluid density and penetration depth in the iron pnictides," *Phys. Rev. B* **79**, 140507 (R) (2009).

[65]. R. T. Gordon, N. Ni, C. Martin, M. A. Tanatar, M.D. Vannette, H. Kim, G. D. Samolyuk, J. Schmalian, S. Nandi, A. Kreyssig, A. I. Goldman, J. Q. Yan, S. L. Bud'ko, P. C. Canfield, and R. Prozorov, "Unconventional London Penetration Depth in Single-Crystal $Ba(Fe_{0.93}Co_{0.07})_2As_2$ Superconductors," *Phys. Rev. B* **102**, 127004 (2009).

[66]. C. Martin, H. Kim, R. T. Gordon, N. Ni, V. G. Kogan, S. L. Bud'ko, P. C. Canfield, M. A. Tanatar, and R. Prozorov, "Evidence from anisotropic penetration depth for a three-dimensional nodal superconducting gap in single-crystalline $Ba(Fe_{1-x}Ni_x)_2As_2$," *Phys. Rev. B* **81**, 060505 (R) (2010).

[67]. R. T. Gordon, H. Kim, M. A. Tanatar, R. Prozorov, and V. G. Kogan, "London penetration depth and strong pair breaking in iron-based superconductors," *Phys. Rev.* **81**, 180501 (R) (2010).

[68]. H. Kim, C. Martin, R. T. Gordon, M. A. Tanatar, J. Hu, B. Qian, Z. Q. Mao, Rongwei Hu, C. Petrovic, N. Salovich, R. Giannetta, and R. Prozorov, "London penetration depth and superfluid density of single-crystalline $Fe_{1+y}(Te_{1-x}Se_x)$ and $Fe_{1+y}(Te_{1-x}S_x)$," *Phys. Rev. B* **81**, 180503 (R) (2010).

[69]. H. Kim, R. T. Gordon, M. A. Tanatar, J. Hua, U. Welp, W. K. Kwok, N. Ni, S. L. Bud'ko, P. C. Canfield, A. B. Vorontsov, and R. Prozorov, "London penetration depth in $Ba(Fe_{1-x}T_x)_2As_2$ (T=Co, Ni) superconductors irradiated with heavy ions," *Phys. Rev. B* **82**, 060518(R) (2010).

[70]. R Prozorov and V G Kogan, "London Penetration Depth in Iron-Based Superconductors," *Rep. Prog. Phys.* **74**, 124505 (2011).

[71]. R. F. Wang, S. P. Zhao, G. H. Chen, and Q. S. Yang, "Absolute Measurement of Penetration Depth in A Superconducting Film by The Two-Coil Technique," *Appl. Phys. Lett.* **75**, 3865 (1999).

[72]. Philipp Gegenwart, Qimiao Si, and Frank Steglich, "Quantum Criticality In Heavy-Fermion Metals," *Nat. Phys.* **4**, 186 (2008).

[73]. Jeffrey M. McMahon, Miguel A. Morales, Carlo Pierleoni, and David M. Ceperley, "The Properties of Hydrogen And Helium Under Extreme Conditions," *Rev. Mod. Phys.* **84**, 1607 (2012).

[74]. Ranga P. Dias and Issac F. Silvera, "Metallic Hydrogen Finally Made In Lab At Mind-Boggling Pressure," *Sci.* **26**. 1579 (2017).

[75]. Walter Greiner, Ludwig Neise, and Horst Stocker, *Thermodynamics And Statistical Mechanics* (Springer, 2nd ed., New York, 1995).

[76]. A. Andreone, A. Cassinese, M. Iavarone, R. Vaglio, I. I. Kulik, and V. Palmieri, "Relation between Normal-State and Superconductive Properties of Sputtered Niobium Films," *Phys. Rev. B* **52**, 4473, (1995).